# Simulation of buoyancy-driven flows in a vertical cylinder using a simple lattice Boltzmann model

Sheng Chen,[*] Jonas Tölke,[†] and Manfred Krafczyk[‡]

*Institute for Computational Modeling in Civil Engineering, Technical University, Braunschweig 38106, Germany*
(Received 13 October 2008; published 12 January 2009)

Axisymmetric thermal flow is of fundamental interest and practical importance. However, the work to design suitable and efficient lattice Boltzmann models on axisymmetric thermal flows is quite rare. In order to bridge the gap, a simple lattice Boltzmann model for axisymmetric thermal flow is proposed in this paper. In the present study, we show how to transform the governing equation for temperate field in the cylindrical coordinate system to the pseudo-Cartesian representation in the same way as that for the flow field. Therefore the flow field and the temperature field both are solved by the two-dimensional five-speed (D2Q5) lattice Boltzmann model. The treatment of the "geometrical forcing" due to the coordinate transformation and the physical forcing due to the temperature field is simpler than that in all existing models. Thanks to its intrinsic features, the present model is more efficient, more stable, and much simpler than the existing models. In this paper, several kinds of nontrivial thermal buoyancy-driven flows in vertical cylinders, which are of interest from the standpoint of both basic fluid dynamics and practical applications, are simulated by the present model.

## I. INTRODUCTION

In the last two decades, the lattice Boltzmann (LB) models have matured as an efficient alternative for simulating and modeling complicated physical, chemical, and social systems [1–23]. The implementation of a LB procedure is quite easy. Parallelization of a LB model is natural since the relaxation is local and the communication pattern in propagation is one way, and the performance increases nearly linearly with the number of CPUs. Moreover, the LB moldes have been compared favorably with spectral methods [24], artificial compressibility methods [25], finite volume methods [26,27], and finite difference methods [28], all quantitative results further validate excellent performance of the LB method not only in computational efficiency but also in numerical accuracy. Due to these advantages, the LB method has been successfully used to simulate many problems, from laminar single phase flows to turbulent multiphase flows [3,4]. For example, the LB method has been widely used for simulating particulate suspensions [19–22] and flexible bodies in flows [23]. In the LB method, the spatial and velocity phases are discretized by the so-called *DdQb* lattice model, where *b* denotes discretized fluid particle speeds and *d* represents lattice dimension [1].

Axisymmetric thermal flows, for which thermal buoyancy-driven flows in vertical cylinders are the representations, represent numerous important flow problems in practice as well as in fundamental [29–34]. Generally, a three-dimensional axisymmetric thermal flow can be reduced to a quasi-two-dimensional problem for traditional computational fluid dynamics (CFD) solvers in the cylindrical coordinate system. However, because the standard LB models are based on the Cartesian coordinate system, therefore we have to use a three-dimensional LB model to solve such quasi-two-

dimensional problems, in which the cubic lattices and a treatment of curved boundary are used. This implies that one or more dimensional lattices are required for simulation of the flows and hence the efficiency is significantly reduced. Therefore an axisymmetric thermal LB model which will only depend on two coordinates, is highly desirable. But, until now the available current literature on axisymmetric thermal lattice Boltzmann models, is still quite rare. To the best knowledge of the present authors, until now there are only two publications [35,39] discussing using axisymmetric LB models to simulate axisymmetric thermal flows.

The first attempt using an axisymmetric LB model to simulate thermal flows was conducted by Peng and his co-workers [35]. They extended Halliday's model [36], which was designed for axisymmetric athermal flow, to simulate Czochralski crystal growth. The spirit of Halliday's model is [36] through the coordinate transformation, the Navier-Stokes equations in the cylindrical coordinate system can be transformed to the specific pseudo-Cartesian representations with "geometrical forcing" terms and then to design a so-called "axisymmetric" LB model to simulate such specific pseudo-Cartesian representations. The outstanding advantage of Halliday's model is that one can use two-dimensional lattice models, such as the two-dimensional nine-speeds (D2Q9) model, to simulate quasi-two-dimensional axisymmetric flows. Comparing with three-dimensional LB models, Halliday's model significantly decreases the computational demand required for such flows [37]. But at the same time, the fairly complex differential expressions in the source terms of the lattice evolution equations, which result from the extremely complicated "geometrical forcing" terms, significantly hamper the numerical stability and computational efficiency of the axisymmetric LB model [38], though there have been many efforts trying to reduce the intrinsic negative effect of Halliday-type LB models [39–43]. The model for axisymmetric thermal flows proposed by Peng *et al.* is a hybrid scheme, namely, to solve the axial and radial velocity components by the Halliday-type axisymmetric LB model and to solve the azimuthal velocity and the temperature by

---
[*]chen@irmb.tu-bs.de
[†]toelke@irmb.tu-bs.de
[‡]kraft@irmb.tu-bs.de

the central difference scheme [35]. The authors used the hybrid scheme to simulate the Wheeler benchmark problem for Czochralski crystal growth, which is an important generic problem investigated both experimentally and computationally [35]. However, because they were hampered by the numerical instability of the hybrid scheme, their discussion was limited in a very narrow range with low values of the Reynolds number and the Grashof number. It was found that the hybrid LB scheme proposed by Peng *et al.* is unstable for simulations of axisymmetric thermal flows with high Reynolds number or high Grashof number even with very fine grid resolutions [39]. Recently, Huang *et al.* proposed an improved version of Peng's model for axisymmetric thermal flows [39]. In Huang's model, an incompressible lattice D2Q9 model is used instead of the standard lattice D2Q9 model in Peng's scheme to improve the numerical stability. In their work, the influence of "geometrical forcing" terms, which caused by the coordinate transformation, on numerical stability and computational efficiency was discussed in detail and the numerical results were compared with those obtained by the quadratic upstream interpolation for convective kinematics (QUICK) scheme. Although Huang's hybrid LB scheme is more numerically stable than Peng's, due to the intrinsic disadvantages of the Halliday-type model, too many complicated force terms existing in Huang's model and a great deal of lattice grids are still required for numerical stability [38,39,44], which means a huge demand of computational resources and makes the improved hybrid LB scheme too expensive to simulate practical cases. Moreover, if there exists additional internal or external forcing, the calculating process of these models will become more complicated because the fluid velocity and the equilibrium velocity both have to be redefined [38,44,45].

In order to overcome the above disadvantages, in this paper a novel and simple axisymmetric thermal LB model, which is an extension of the model designed in our previous work [44], is proposed to simulate axisymmetric thermal flows. In the present study, we show how to transform the governing equation for temperate field in the cylindrical coordinate system to the pseudo-Cartesian representation in the same way as that for the flow field. There are two main differences between the present model and the existing axisymmetric LB models for axisymmetric thermal flows [35,39]: First, in the present scheme, the flow field and the temperature field both are solved by the two-dimensional five-speeds (D2Q5) lattice model. Second, for flow field, the target macroscopic equations of the present model are vorticity-stream-function equations instead of the primitive-variables-based Navier-Stokes equations. The first characteristic makes the present model keep the simplicity of code, which is an attractive advantage for both practitioners and novices. The second characteristic makes the present model more stable and more efficient than the existing models. In the present model, the source terms caused by the coordinate transformation are simpler and less than that in all existing Halliday-type axisymmetric LB models [35,36,39–43], without any complex terms. Generally speaking, adding complex position and time-dependent source terms into LB models would decrease the numerical stability besides computational efficiency [39]. Furthermore, because the vorticity-stream-

function equations consist of an advection-diffusion equation and a Poisson equation, for which the source terms in the LB models can be treated more simply than the force strategy for the primitive-variables-based LB equation with additional forcing(see Refs. [7,45,44]). Consequently compared with both Halliday-type axisymmetric LB models [35,36,39–43] and the non-Halliday-type axisymmetric athermal LB model recently developed by Zhou [38], the computation process is simplified and the computational efficiency is improved in the present model because in this model the treatment of the "geometrical forcing" due to the coordinate transformation and the physical forcing due to the temperature field is simpler than that in all existing models, avoiding redefining the fluid velocity and the equilibrium velocity together with avoiding the expansion of forcing in a power series in the particle velocity [44,45]. From the point of numerical analysis, vorticity-stream-function-based equations themselves are more suitable and more efficient than primitive-variables-based ones for axisymmetric thermal flows, especially for the cases with high Reynolds number and high Grashof number [49]. And the stream function, which can figure out the character of flow, can be solved directly.

The rest of the paper is organized as follows. Vorticity-stream-function-based governing equations for axisymmetric thermal flows is presented in Sec. II. In Sec. III, a novel and simple axisymmetric thermal LB model is introduced. In Sec. IV, numerical experiments are performed to validate the present model. Summary and conclusion are presented in Sec. V.

## II. GOVERNING EQUATIONS FOR AXISYMMETRIC THERMAL FLOWS

With the Boussinesq assumption, the primitive-variables-based governing equations for axisymmetric thermal flows in the cylindrical coordinate system can be written as [29–34]

$$\frac{1}{r}\frac{\partial(ru)}{\partial r} + \frac{\partial w}{\partial z} = 0, \tag{1}$$

$$\frac{\partial u}{\partial t} + u\frac{\partial u}{\partial r} + w\frac{\partial u}{\partial z} = -\frac{1}{\rho}\frac{\partial p}{\partial r} + \nu\nabla^2 u, \tag{2}$$

$$\frac{\partial w}{\partial t} + u\frac{\partial w}{\partial r} + w\frac{\partial w}{\partial z} = -\frac{1}{\rho}\frac{\partial p}{\partial z} + \nu\nabla^2 w + g\alpha\Delta T, \tag{3}$$

$$\frac{\partial T}{\partial t} + u\frac{\partial T}{\partial r} + w\frac{\partial T}{\partial z} = \kappa\nabla^2 T, \tag{4}$$

where

$$\nabla^2 = \frac{1}{r}\frac{\partial}{\partial r}\left(r\frac{\partial}{\partial r}\right) + \frac{\partial^2}{\partial z^2}.$$

$u$ and $w$ are radial and axial velocity components, $p$ is the pressure, $T$ is the temperature, $\nu$ is the kinetic viscosity, $g$ is the gravitational acceleration along the negative $z$ axis, $\kappa$ is the thermal conductivity, $\rho$ is the density, $\Delta T$ is the temperature difference, and $\alpha$ the coefficient of thermal expansion.

For axisymmetric flow, computation time can be reduced if the problem is reformulated so that the three variables $u$, $w$, $p$ are eliminated in favor of the vorticity $\omega$ and Stokes stream function $\psi$ [49], which are defined as

$$\omega = \frac{\partial w}{\partial r} - \frac{\partial u}{\partial z}, \tag{5}$$

$$u = \frac{1}{r}\frac{\partial \psi}{\partial z}, \tag{6}$$

$$w = -\frac{1}{r}\frac{\partial \psi}{\partial r}. \tag{7}$$

The dimensionless vorticity-stream-function-based governing equations read [29–34]

$$\frac{\partial \widetilde{S}}{\partial \widetilde{t}} + \widetilde{u}\frac{\partial \widetilde{S}}{\partial \widetilde{r}} + \widetilde{w}\frac{\partial \widetilde{S}}{\partial \widetilde{z}} = \text{Pr}\frac{1}{\widetilde{r}}\frac{\partial \widetilde{T}}{\partial \widetilde{r}} + \frac{\text{Pr}}{\text{Ra}^{1/2}}\left\{ \frac{1}{\widetilde{r}}\frac{\partial}{\partial \widetilde{r}}\left[ \frac{1}{\widetilde{r}}\frac{\partial}{\partial \widetilde{r}}(\widetilde{r}^2\widetilde{S}) \right] \right. $$
$$\left. + \frac{\partial^2 \widetilde{S}}{\partial \widetilde{z}^2} \right\}, \tag{8}$$

$$\frac{\partial \widetilde{T}}{\partial \widetilde{t}} + \widetilde{u}\frac{\partial \widetilde{T}}{\partial \widetilde{r}} + w\frac{\partial \widetilde{T}}{\partial \widetilde{z}} = \frac{1}{\text{Ra}^{1/2}}\left[ \frac{1}{\widetilde{r}}\frac{\partial}{\partial \widetilde{r}}\left(\widetilde{r}\frac{\partial \widetilde{T}}{\partial \widetilde{r}}\right) + \frac{\partial^2 \widetilde{T}}{\partial \widetilde{z}^2} \right], \tag{9}$$

$$\frac{\partial}{\partial \widetilde{r}}\left( \frac{1}{\widetilde{r}}\frac{\partial \widetilde{\psi}}{\partial \widetilde{r}} \right) + \frac{1}{\widetilde{r}}\frac{\partial^2 \widetilde{\psi}}{\partial \widetilde{z}^2} = -\widetilde{r}\widetilde{S}. \tag{10}$$

In the above equations the parameters with tildes represent the dimensionless counterparts. We omit the tildes from this point forward for clarity. $S = \omega/r$ is the Svanberg vorticity for numerically stable modeling of physically unstable flows [49]. The Prandtl number $\text{Pr} = \nu/\kappa$ and the Rayleigh number $\text{Ra} = \alpha g R^3 \Delta T/\nu\kappa$. $R$ is the characteristic length.

## III. COORDINATE TRANSFORMATION AND AXISYMMETRIC THERMAL LATTICE BOLTZMANN MODEL

By performing the following coordinate transformation [35,39,44]:

$$(r,z) \mapsto (x,y), \tag{11}$$

$$(u,w) \mapsto (u,v). \tag{12}$$

Equations (6)–(10) can be written in the pseudo-Cartesian coordinates

$$u = \frac{1}{x}\frac{\partial \psi}{\partial y}, \tag{13}$$

$$v = -\frac{1}{x}\frac{\partial \psi}{\partial x}, \tag{14}$$

$$\frac{\partial S}{\partial t} + u\frac{\partial S}{\partial x} + v\frac{\partial S}{\partial y} = \frac{\text{Pr}}{\text{Ra}^{1/2}}\left( \frac{\partial^2 S}{\partial x^2} + \frac{\partial^2 S}{\partial y^2} \right) + S_o, \tag{15}$$

$$\frac{\partial T}{\partial t} + u\frac{\partial T}{\partial x} + v\frac{\partial T}{\partial y} = \frac{1}{\text{Ra}^{1/2}}\left( \frac{\partial^2 T}{\partial x^2} + \frac{\partial^2 T}{\partial y^2} \right) + T_o, \tag{16}$$

$$\frac{\partial^2 \psi}{\partial y^2} + \frac{\partial^2 \psi}{\partial x^2} = \Theta. \tag{17}$$

In Eqs. (15)–(17), the source terms caused by the coordinate transformation and the buoyant forcing due to the temperature read

$$S_o = \frac{3}{x}\frac{\text{Pr}}{\text{Ra}^{1/2}}\frac{\partial S}{\partial x} + \text{Pr}\frac{1}{x}\frac{\partial T}{\partial x}, \tag{18}$$

$$T_o = \frac{1}{\text{Ra}^{1/2}}\frac{1}{x}\frac{\partial T}{\partial x}, \tag{19}$$

$$\Theta = -(x^2 S + v). \tag{20}$$

Bearing in mind that from now on $u$ and $v$ stand for the velocity components along $x$ and $y$ coordinates.

Equation (15) (governing equation for the flow field) and Eq. (16) (governing equation for the temperature field), which have the same formulation except different coefficients, are nothing but advection-diffusion equations with source terms. There are many matured efficient lattice Boltzmann models for this type of equation [44]. In this paper a D2Q5 model is employed to solve these equations. It reads

$$g_k(\vec{x} + c\vec{e}_k\Delta t, t+\Delta t) - g_k(\vec{x},t) = -\tau^{-1}[g_k(\vec{x},t) - g_k^{(eq)}(\vec{x},t)]$$
$$+ \Delta t \Upsilon_{o,k}, \tag{21}$$

where $\vec{e}_k$ $(k=0-4)$ are the discrete velocity directions

$$\vec{e}_k = \begin{cases} (0,0): & k=0, \\ [\cos(k-1)\pi/2, \sin(k-1)\pi/2]: & k=1,2,3,4, \end{cases}$$

$c = \Delta x/\Delta t$ is the fluid particle speed. $\Delta x$, $\Delta t$, and $\tau$ are the lattice grid spacing, the time step and the dimensionless relaxation time, respectively. $\Upsilon_{o,k}$ is the discrete form of the source term $\Upsilon_o$ [7,44], $\Upsilon_o = S_o, T_o$ for Eqs. (15) and (16), respectively. $\Upsilon_{o,k}$ satisfies

$$\sum_{k\geq 0} \Upsilon_{o,k} = \Upsilon_o. \tag{22}$$

The simplest choice satisfying the constraint (22) is

$$\Upsilon_{o,k} = \frac{\Upsilon_o}{5}. \tag{23}$$

Compared with the existing axisymmetric LB models, either for thermal flows [35,39] or for athermal ones [36,38,40–43], the expression of $\Upsilon_{o,k}$ in the present model is the simplest one, without any complex term.

The equilibrium distribution $g_k^{(eq)}$ is defined by

$$g_k^{(eq)} = \frac{\delta}{5}\left[ 1 + 2.5\frac{\vec{e}_k \cdot \vec{u}}{c} \right]. \tag{24}$$

$\delta = S, T$ for Eqs. (15) and (16), respectively, and is obtained by

$$\delta = \sum_{k \geq 0} g_k \qquad (25)$$

and the dimensionless relaxation time $\tau$ is determined by

$$\chi = \frac{2c^2(\tau - 0.5)}{5}, \qquad (26)$$

$\chi = \frac{\text{Pr}}{\text{Ra}^{1/2}}, \frac{1}{\text{Ra}^{1/2}}$ for Eqs. (15) and (16), respectively.

In theory one can use other lattice models, for example the D2Q9 lattice model, to solve Eqs. (15) and (16). But the D2Q5 one perhaps is the best choice for the present approach, in which the collision term is Bhatnagar-Gross-Krook (BGK) formation [1]. There are at least two advantages of the D2Q5-BGK model over others: First, the computational cost of the D2Q5-BGK model is the lowest, and second, under low Mach number condition, the D2Q5-BGK model receives smaller influence of viscosity-dependent error than other BGK-type lattice models [46–48].

Another comment with regard to the present model also should be pointed out: there are viscosity-dependent errors in lattice BGK models. This disadvantage can be overcame by lattice-two-relaxation-times (TRT) models proposed by Ginzburg *et al.* [46,50,51].

Equation (17) is just the Poisson equation, which also can be solved by the LB method efficiently. In the present study, the D2Q5 model used in our previous work [44] is employed because this model is more efficient and more accurate than others to solve the Poisson equation. The evolution equation for Eq. (17) reads

$$f_k(\vec{x} + c\vec{e}_k \Delta t, t + \Delta t) - f_k(\vec{x}, t) = \Omega_k + \Omega_k', \qquad (27)$$

where $\Omega_k = -\tau_\psi^{-1}[f_k(\vec{x}, t) - f_k^{(eq)}(\vec{x}, t)]$, $\Omega_k' = \Delta t \zeta_k \Theta D$ and $D = \frac{c^2}{2}(0.5 - \tau_\psi)$. $\tau_\psi > 0.5$ is the dimensionless relaxation time [44]. $f_k^{(eq)}$ is the equilibrium distribution function, and defined by

$$f_k^{(eq)} = \begin{cases} (\xi_0 - 1.0)\psi: & k = 0, \\ \xi_k \psi: & k = 1, 2, 3, 4. \end{cases}$$

$\xi_k$ and $\zeta_k$ are weight parameters given as $\xi_0 = \zeta_0 = 0$, $\xi_k = \zeta_k = 1/4(k = 1-4)$. $\psi$ is obtained by

$$\psi = \sum_{k \geq 1} f_k. \qquad (28)$$

The detailed derivation from Eqs. (21) and (27) to Eqs. (15)–(17) can be found in the Appendix. In the present model Eqs. (13) and (14) and the differential terms in Eqs. (18) and (19) are solved by the central finite difference scheme.

## IV. NUMERICAL RESULTS

In the present study, three different kinds of nontrivial thermal buoyancy-driven flows in vertical cylindrical enclosures are considered to validate the present model. They share the same physical configuration but with different boundary conditions. Figure 1 illustrates the computational domain with the aspect ration $\Lambda = H/R$. $H$ is the height of the vertical cylinder and $R$ is the radius. In the present study, $\Lambda = 1.0$ for all cases.
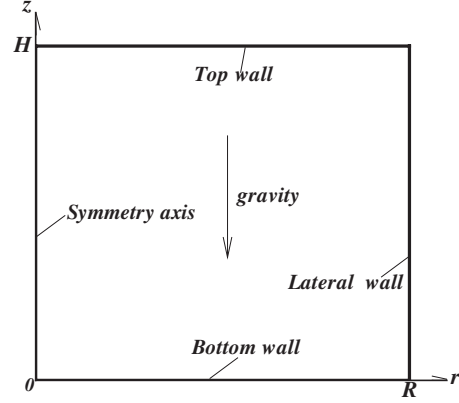


FIG. 1. The configuration of computational domain.

The first case is Rayleigh-Bénard convection in a vertical cylinder, where a fluid layer is heated from below, cooled at its upper surface and laterally insulated. Due to its practical importance in many general science and engineering applications, Rayleigh-Bénard convection has been the subject of many theoretical, experimental, and numerical studies [52–55]. However, nearly all existing simulations on Rayleigh-Bénard convection using LB models are limited in planar rectangular domains [56–58], though the counterpart in a vertical cylinder is more fundamental. In the present study, the setting in Ref. [30] is adopted: namely, the fluid in the cylinder is heated form below by the bottom wall with temperature $T = 1.0$ and cooled from above by the top wall with temperature $T = 0.0$; the lateral wall is insulated and no-slip conditions are assumed at all walls; along the symmetry, the axisymmetric boundary condition is adopted, i.e., $\frac{\partial u}{\partial r} = 0$, $v = 0$, $\frac{\partial T}{\partial r} = 0$, and $S = 0$; Ra=5000 and Pr=0.7. The stream function is assumed $\psi = 0$ at all walls. The values of Svanberg vorticity $S$ at all walls are calculated according to the method used in our previous study [44].

The second case is natural convection in a laterally heated and upper cooled vertical cylinder, which is of great fundamental and practice interest to understand convection phenomena in energy storage systems. There are very few studies on it, which all conducted with the traditional CFD methods [30,59]. In the present study, natural convection in a laterally heated and upper cooled vertical cylinder is investigated with $10^3 \leq \text{Ra} \leq 10^5$ and Pr=0.7. The initial conditions are $\psi = 0$, $S = 0$, and $T = 0$. The axisymmetric boundary condition is adopted for the symmetry. The bottom is insulated. The lateral wall is heated due to the imposed fixed heat flux $\frac{\partial T}{\partial r} = 1$ while the top is cooled with $\frac{\partial T}{\partial z} = -4$. No-slip conditions and $\psi = 0$ are assumed at all walls. The configuration is the same as that in Ref. [30].

The third case is very similar with the second one except the fluid in the vertical cylinder is cooled at the lateral wall due to the imposed fixed wall temperature while the top and bottom are insulated. The transient unsteady evolving process of cooling down in such configuration has attracted many interests due to its practical importance [31,59]. In the present study, the transient process after suddenly changing the temperature at the lateral wall from $T = 0$ to $T = -1$ is investigated with $10^6 \leq \text{Ra} \leq 10^8$ and Pr=7.

TABLE I. Top and bottom average Nusselt number.

| | Ref. [30] | Present ($100 \times 100$) | Present ($200 \times 200$) |
|---|---|---|---|
| $Nu_b$ | 4.442 | 4.246 | 4.202 |
| $Nu_t$ | 4.561 | 4.359 | 4.362 |

### A. Rayleigh-Bénard convection in a vertical cylinder

Grid resolutions $100 \times 100$ and $200 \times 200$ were used for Rayleigh-Bénard convection in a vertical cylinder with Ra $=5000$. We found the former was fine enough to obtain the average Nusselt number $Nu_b$ at the bottom nearly identical to the average Nusselt number $Nu_t$ at the top (conservation of the energy). To quantify the results, the average Nusselt number $Nu_b$ at the bottom and $Nu_t$ at the top obtained by the present model are listed in Table I, with that obtained by the ADI method in Ref. [30]. In the table, the number in the bracket indicates the grid size used. The results obtained by the present model agree well with that in Ref. [30].

In this case Ra$=5000$ is big enough to produce obvious disturbance. Figures 2 and 3 illustrate the isothermal and streamfunction contours obtained by the present model. Toroidal rolls appear in the domain because the fluid near the opposite sides has opposite velocity direction. There are two interesting features of the flow under the conditions [30]: setting initial temperatures to zero everywhere induces an upflow at the center of the cylinder, while if buoyancy is increased by initial conditions, for instance with an initial hot penultimate column of the computational domain, a downflow is induced at the center, as shown in Figs. 2 and 3. It can also be seen that the center of the toroidal roll is slightly shifted upwards in the case of upflow and downwards in the case of downflow. This asymmetry encountered by previous studies (Ref. [30], and references therein) can be captured by the present model clearly.

### B. Natural convection in a laterally heated and upper cooled vertical cylinder

A $100 \times 100$ uniform grid is used for simulations of natural convection in a laterally heated and upper cooled vertical cylinder, with $10^3 \leqslant$ Ra $\leqslant 10^5$ and Pr$=0.7$. As Figs. 4–6 show, in all cases studied, the flow presents toroidal rolls. At low Ra, near a conductive regime, the isotherms are slightly
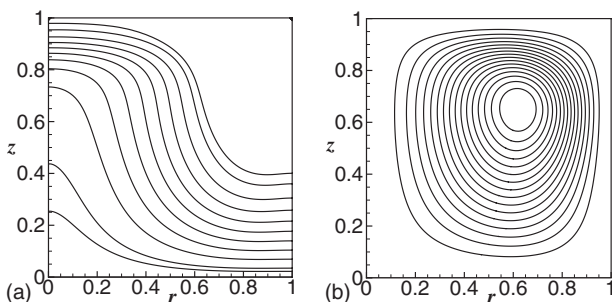


FIG. 2. Isothermal (a) and stream function (b) contours of Rayleigh-Bénard convection at Ra$=5000$ and Pr$=0.7$: upflow at the symmetry axis.
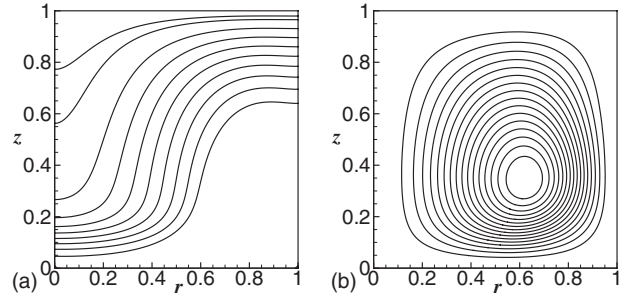


FIG. 3. Isothermal (a) and stream function (b) contours of Rayleigh-Bénard convection at Ra$=5000$ and Pr$=0.7$: downflow at the symmetry axis.

deformed by the movement, with the highest temperature in the lower corner of the cylinder. As Ra increases, the isotherms become much more deformed with a clear homogenization of the hot area along the sidewall due to the upward buoyancy-induced flow. The maximum velocity is enhanced with Ra increasing, as listed in Table II, with that published in Ref. [30]. Table III shows the top average Nusselt number $Nu_t$ and lateral average Nusselt number $Nu_l$ versus the Rayleigh number Ra, compared with that in Ref. [30]. The results obtained by the present model still agree well with that in the previous study [30].

### C. Transient process in a laterally cooled vertical cylinder

A $100 \times 100$ uniform grid is used for simulating the transient process, namely, the growth of the vertical thermal boundary layer on the sidewall and the movement of the horizontal intrusion [31]. Initially, the temperature of the fluid in the vertical cylinder is zero everywhere. At time $t$ $=0$, after the temperature at the lateral wall is suddenly changed to $-1$, a vertical thermal boundary layer on the sidewall appears and grows. After the thermal boundary layer is fully developed, the intrusion generated at the downstream end of the boundary layer travels across the domain from the cooled wall to the symmetry axis, as Fig. 7 illustrates. The maximum nondimensionalized thicknesses of the vertical thermal boundary layers $d_s$ at full development and the nondimensional time $t_s$ for the intrusion layer to arrive at the symmetry axis are shown in Figs. 8 and 9, versus Ra. Some features can been seen immediately from these figures. One is that the thickness of the horizontal viscous intrusions in-
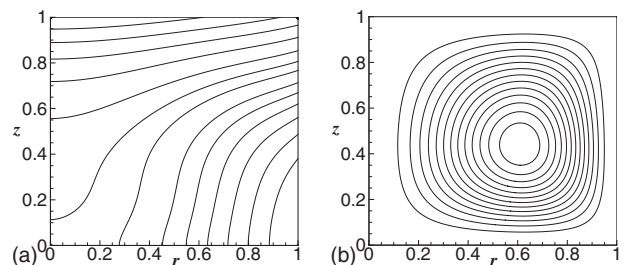


FIG. 4. Isothermal (a) and stream function (b) contours of natural convection in the laterally heated and upper cooled vertical cylinder at Ra$=10^3$ and Pr$=0.7$.
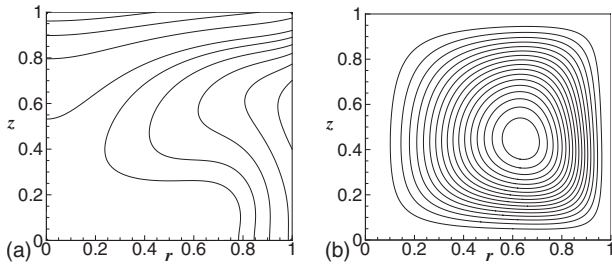
FIG. 5. Isothermal (a) and stream function (b) contours of natural convection in the laterally heated and upper cooled vertical cylinder at Ra$=10^4$ and Pr$=0.7$.

crease as they move towards the symmetry axis. The second feature is that the thicknesses of the thermal boundary layer becomes smaller when Ra increases. The third one is that the nondimensional time for the intrusion layer to arrive at the symmetry axis becomes longer when Ra increases. All these observations obtained by the present model agree well again with that predicted in Ref. [31].

## V. CONCLUSION

Axisymmetric thermal flow is of fundamental interest and practical importance. But the work to design a suitable and efficient LB model on it is rare, which inspirits the present study. In this paper we proposed a simple axisymmetric thermal LB model to bridge the gap. Unlike previous models for axisymmetric thermal flow, which based on "primitive-variables" Navier-Stokes equations, the target macroscopic equations of the present model for the flow field are vorticity-stream-function equations. In the present study, we show how to transform the governing equation for temperate field in the cylindrical coordinate system to the pseudo-Cartesian representation in the same way as that for the flow field. Benefitting from its intrinsic features, in the present model the "geometrical forcing" due to the axisymmetric contributions and the physical buoyant forcing due to the temperature field just need to be expanded to first order and the constraint on its discrete form is very simple, without any spatially differential term or complex term. And the complicated process of redefining the fluid velocity and the equilibrium velocity together with the expansion of forcing in a power series in the particle velocity, which appear in the existing primitive-variables-base axisymmetric LB models,
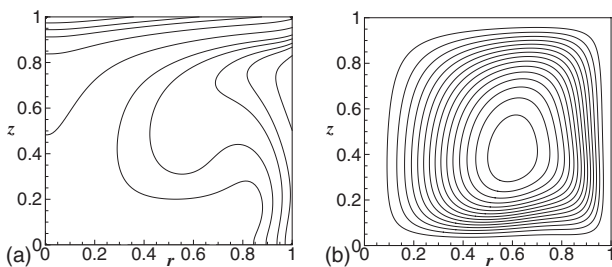


FIG. 6. Isothermal (a) and stream function (b) contours of natural convection in the laterally heated and upper cooled vertical cylinder at Ra$=10^5$ and Pr$=0.7$.

TABLE II. Maximum velocity versus Rayleigh number.

| Ra | Ref. [30] | Present |
|----|-----------|---------|
| $10^3$ | 0.2391 | 0.2350 |
| $10^4$ | 0.4143 | 0.4075 |
| $10^5$ | 0.4552 | 0.4547 |

are avoided in the present model. Moreover, the D2Q5 lattice model is used for both flow field and temperature field. Therefore the present model is more efficient, more stable and much simpler than the existing models for axisymmetric thermal flow. However, if the physical field is not axisymmetrical, namely, the gradients of azimuthal direction do not equal zero, the present model is invalid.

We first validated the model by simulating Rayleigh-Bénard convection in a vertical cylinder, which has been the subject of many theoretical, experimental, and numerical studies. When the Ra exceeds a certain critical value, disturbance will be enhanced. With different initial conditions, there exist two different kinds of flow patterns. The present model captured the features very well.

We then applied our model to natural convection in a laterally heated and upper cooled vertical cylinder and found again the numerical results obtained by the present model were excellent agreement with that in previous literature. The influence of a little change of Ra on the stream function and isothermal contours is significant.

Finally, the transient process in a laterally cooled vertical cylinder was investigated. The present model can still work well up to Ra$=10^8$ with a low grid resolution.

There exist slight deviations between the results obtained by the present model and that in previous publications, which perhaps result from the viscosity-dependent errors of lattice BGK model. We will try to use the lattice TRT model to answer this question in the future work. Though in this paper the present model only is used to simulate axisymmetric thermal flow without swirl, the extension for modeling the problems of rotational thermal flow is straightforward, which will be considered in future studies.

## ACKNOWLEDGMENTS

TABLE III. Top and lateral average Nusselt number versus Rayleigh number.

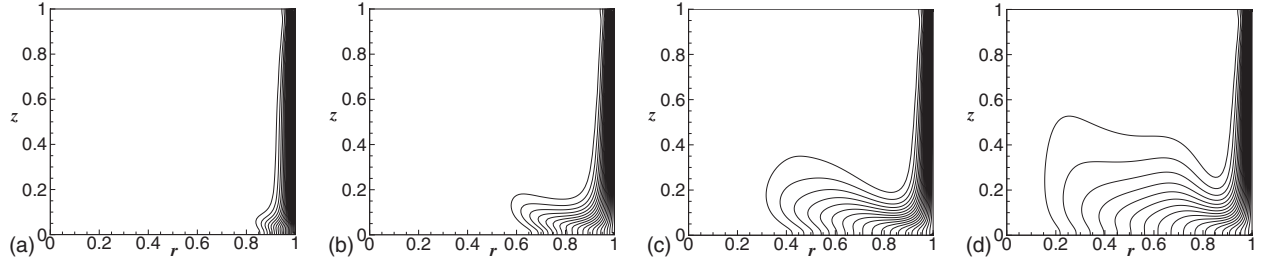| Ra | Nu$_t$ | | Nu$_l$ | |
|----|--------|--------|--------|--------|
| | Ref. [30] | Present | Ref. [30] | Present |
| $10^3$ | 7.4604 | 7.0663 | 6.6698 | 6.2879 |
| $10^4$ | 14.5255 | 14.2291 | 9.5848 | 8.9658 |
| $10^5$ | 24.3568 | 23.9619 | 15.0687 | 14.2782 |

FIG. 7. Isothermal contours of transient process in the laterally cooled vertical cylinder at different time: (a) $t=1$, (b) $t=2$, (c) $t=3$, (d) $t=4$; $Ra=10^6$ and $Pr=7$.

## APPENDIX: RECOVERY OF THE AXISYMMETRIC GOVERNING EQUATIONS

The recovery of the axisymmetric governing equations is aided by the Chapman-Enskog expansion. Expanding the distribution functions and the time and space derivatives in terms of a small quantity $\epsilon$

$$\partial_t = \epsilon \partial_{1t} + \epsilon^2 \partial_{2t}, \quad \partial_\alpha = \epsilon \partial_{1\alpha}, \quad \Upsilon_{o,k} = \epsilon \Upsilon_{o,1k}, \quad (A1)$$

$$g_k = g_k^{(0)} + \epsilon g_k^{(1)} + \epsilon^2 g_k^{(2)} + \cdots .$$

To perform the Chapman-Enskog expansion we must first Taylor expand Eq. (21):

$$\Delta t D_k g_k + \frac{\Delta t^2}{2} D_k^2 g_k = -\frac{1}{\tau}(g_k - g_k^{(eq)}) + \Delta t \Upsilon_{o,k}, \quad (A2)$$

where $D_k = \partial_t + c e_{k,\alpha} \partial_\alpha$. Substituting Eq. (A1) into Eq. (A2), we get

$$\epsilon \Delta t D_{1k}(g_k^{(0)} + \epsilon g_k^{(1)}) + \epsilon^2 \Delta t \partial_{2t} g_k^{(0)} + \epsilon^2 \frac{\Delta t^2}{2} D_{1k}^2 g_k^{(0)}$$

$$= -\frac{1}{\tau}(g_k^{(0)} + \epsilon g_k^{(1)} + \epsilon^2 g_k^{(2)} - g_k^{(eq)}) + \epsilon \Delta t \Upsilon_{o,1k}, \quad (A3)$$

where $D_{1i} = \partial_{1t} + c e_{k,\alpha} \partial_{1\alpha}$. And then, we can obtain the following equations in consecutive order of the parameter $\epsilon$:

$$O(\epsilon^0): g_k^{(0)} = g_k^{(eq)}, \quad (A4a)$$

$$O(\epsilon^1): D_{1k} g_k^{(0)} = -\frac{1}{\tau \Delta t} g_k^{(1)} + \Upsilon_{o,1k}, \quad (A4b)$$

$$O(\epsilon^2): \partial_{2t} g_k^{(0)} + \frac{\Delta t}{2} D_{1k}^2 g_k^{(0)} + D_{1k} g_k^{(1)} = -\frac{1}{\tau \Delta t} g_k^{(2)}. \quad (A4c)$$

Equation (A4c) can be simplified by Eq. (A4b):

$$\partial_{2t} g_k^{(0)} + \left(1 - \frac{1}{2\tau}\right) D_{1k} g_k^{(1)} = -\frac{1}{\tau \Delta t} g_k^{(2)} - \frac{\Delta t}{2} D_{1k} \Upsilon_{o,1k}. \quad (A5)$$

Because

$$\sum_k g_k^{(i)} = 0 \quad i \geq 1,2 \quad (A6)$$

we can obtain

$$\partial_{t1} \delta + u_\alpha \partial_{1\alpha} \delta = \Upsilon_o \quad (A7)$$

and

$$\partial_{t2} \delta + \partial_{1\alpha} \pi_\alpha^{(1)} = 0, \quad (A8)$$

where

$$\pi_\alpha^{(1)} = -\frac{2c^2(\tau - 0.5)}{5} \partial_{1\alpha} \delta + O(\epsilon^2). \quad (A9)$$

Combining Eqs. (A8) and (A9), we can obtain Eqs. (15) and (16) if $\delta = S, T$, respectively. The detailed derivation from Eq. (27) to Eq. (17) can be found in our previous work [44].
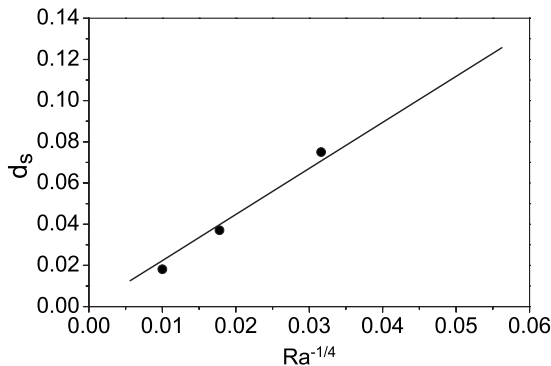


FIG. 8. $d_s$ vs $Ra^{-1/4}$ in the laterally cooled vertical cylinder: dot, present results; line, predicted values in Ref. [31].
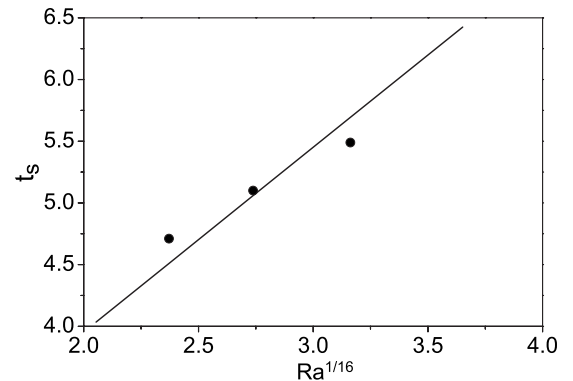


FIG. 9. $t_s$ vs $Ra^{1/16}$ in the laterally cooled vertical cylinder: dot, present results; line, predicted values in Ref. [31].

[1] Y. Qian, D. dHumieres, and P. Lallemand, Europhys. Lett. **17**, 479 (1992).

[2] R. Benzi, S. Succi, and M. Vergassola, Phys. Rep. **222**, 145 (1992).

[3] S. Chen and G. D. Doolen, Annu. Rev. Fluid Mech. **30**, 329 (1998).

[4] S. Succi, *The Lattice Boltzmann Equation for Fluid Dynamics and Beyond* (Oxford University Press, Oxford, 2001).

[5] R. J. Goldstein *et al.*, Int. J. Heat Mass Transfer **49**, 451 (2006).

[6] S. Succi, E. Foti, and F. Higuera, Europhys. Lett. **10**, 433 (1989).

[7] S. P. Dawson, S. Chen, G. D. Doolen, D. R. Janecky, and A. Lawniczak, Comput. Chem. Eng. **19**, 617 (1995).

[8] H. Chen, S. Kandasamy, S. Orszag, R. Shock, S. Succi, and V. Yakhot, Science **301**, 633 (2003).

[9] Y. H. Qian, S. Succi, and S. Orszag, in *Annual Reviews of Computational Physics*, Vol. 3, edited by D. Stauffer (World Scientific, Singapore, 1995), pp. 195–242.

[10] G. Hazi *et al.*, Ann. Nucl. Energy **29**, 1421 (2002).

[11] D. Yu *et al.*, Prog. Aerosp. Sci. **39**, 329 (2003).

[12] M. C. Sukop and D. T. Thorne Jr., *Lattice Boltzmann Modeling: An Introduction for Geoscientists and Engineers* (Springer, Heidelberg, 2006).

[13] S. Chakraborty and D. Chatterjee, J. Fluid Mech. **592**, 155 (2007).

[14] S. Chen *et al.*, Int. J. Mod. Phys. C **18**, 187 (2007).

[15] Z. Guo, C. Zheng, and B. Shi, Phys. Rev. E **77**, 036707 (2008).

[16] D. Raabe, Modell. Simul. Mater. Sci. Eng. **12**, R13 (2004).

[17] J. Meng, Y. Qian, X. Li, and S. Dai, Phys. Rev. E **77**, 036108 (2008).

[18] K. Furtado and J. M. Yeomans, Phys. Rev. E **73**, 066124 (2006).

[19] A. J. C. Ladd, J. Fluid Mech. **271**, 311 (1994).

[20] C. K. Aidun, Y. Lu, and E. Ding, J. Fluid Mech. **373**, 287 (1998).

[21] D. Qi and L. Luo, J. Fluid Mech. **477**, 201 (2003).

[22] J. Derksen and S. Sundaresan, J. Fluid Mech. **587**, 303 (2007).

[23] D. Qi, J. Chem. Phys. **125**, 114901 (2006).

[24] D. O. Martinez *et al.*, Phys. Fluids **6**, 1285 (1994).

[25] X. He, G. D. Doolen, and T. Clark, J. Comput. Phys. **179**, 439 (2002).

[26] Y. Y. Al-Jahmany, G. Brenner, and P. O. Brunn, Int. J. Numer. Methods Fluids **46**, 903 (2004).

[27] A. Al-Zoubi and G. Brenner, Int. J. Mod. Phys. C **15**, 307 (2004).

[28] T. Seta, E. Takegoshi, and K. Okui, Math. Comput. Simul. **72**, 195 (2006).

[29] D. R. Otis, Int. J. Heat Mass Transfer **30**, 1633 (1987).

[30] A. Lemembre and J. P. Petit, Int. J. Heat Mass Transfer **41**, 2437 (1998).

[31] W. Lin and S. W. Armfield, Int. J. Heat Fluid Flow **22**, 72 (2001).

[32] G. Neumann, J. Fluid Mech. **214**, 559 (1990).

[33] R. S. Figliola, Phys. Fluids **29**, 2028 (1986).

[34] S. F. Liang, A. Vidal, and A. Acrivos, J. Fluid Mech. **36**, 239 (1969).

[35] Y. Peng, C. Shu, Y. T. Chew, and J. Qiu, J. Comput. Phys. **186**, 295 (2003).

[36] I. Halliday, L. A. Hammond, C. M. Care, K. Good, and A. Stevens, Phys. Rev. E **64**, 011208 (2001).

[37] S. K. Bhaumik and K. N. Lakshmisha, Comput. Fluids **36**, 1163 (2007).

[38] J. G. Zhou, Phys. Rev. E **78**, 036701 (2008).

[39] H. Huang, T. S. Lee, and C. Shu, Int. J. Numer. Methods Fluids **53**, 1707 (2007).

[40] T. Reis and T. N. Phillips, Phys. Rev. E **75**, 056703 (2007).

[41] T. Reis and T. N. Phillips, Phys. Rev. E **77**, 026703 (2008).

[42] T. S. Lee, H. Huang, and C. Shu, Int. J. Numer. Methods Fluids **49**, 99 (2005).

[43] T. S. Lee, H. Huang, and C. Shu, Int. J. Mod. Phys. C **17**, 645 (2006).

[44] S. Chen, J. Tolke, S. Geller, and M. Krafczyk, Phys. Rev. E **78**, 046703 (2008).

[45] Z. Guo, C. Zheng, and B. Shi, Phys. Rev. E **65**, 046308 (2002).

[46] I. Ginzburg, Comm. Comp. Phys. **3**, 519 (2008).

[47] B. Servan-Camas and F. Tsai, Adv. Water Resour. **31**, 1113 (2008).

[48] B. Servan-Camas and F. Tsai, J. Comput. Phys. **228**, 236 (2009).

[49] W. E. Langlois, Annu. Rev. Fluid Mech. **17**, 191 (1985).

[50] I. Ginzburg, Adv. Water Resour. **28**, 1171 (2005).

[51] I. Ginzburg, F. Verhaeghe, and D. d'Humieres, Comm. Comp. Phys. **3**, 427 (2008).

[52] E. Brown and G. Ahlers, Phys. Rev. Lett. **98**, 134501 (2007).

[53] X. D. Shang, P. Tong, and K. Q. Xia, Phys. Rev. Lett. **100**, 244503 (2008).

[54] G. Neumann, J. Fluid Mech. **214**, 559 (1990).

[55] E. Bodenschatz, W. Pesch, and G. Ahlers, Annu. Rev. Fluid Mech. **32**, 709 (2000).

[56] X. Shan, Phys. Rev. E **55**, 2780 (1997).

[57] X. He, S. Chen, and G. D. Doolen, J. Comput. Phys. **146**, 282 (1998).

[58] P. H. Kao and R. J. Yang, Int. J. Heat Mass Transfer **50**, 3315 (2007).

[59] W. Lin and S. W. Armfield, Int. J. Heat Mass Transfer **48**, 53 (2005).